Physics Letters B 705 (2011) 87–92

Contents lists available at SciVerse ScienceDirect

Physics Letters B

www.elsevier.com/locate/physletb

LHC constraints on NLSP gluino and dark matter neutralino in Yukawa unified models

M. Adeel Ajaib, Tong Li *, Qaisar Shafi

Bartol Research Institute, Department of Physics and Astronomy, University of Delaware, Newark, DE 19716, USA

ARTICLE INFO

Article history:
Received 25 July 2011
Received in revised form 14 September 2011
Accepted 21 September 2011
Available online 1 October 2011
Editor: M. Cvetič

ABSTRACT

The ATLAS experiment has recently presented its search results for final states containing jets and/or b-jet(s) and missing transverse momentum, corresponding to an integrated luminosity of 165 pb^{-1}. We employ this data to constrain a class of supersymmetric $SU(4)_c \times SU(2)_L \times SU(2)_R$ models with $t-b-\tau$ Yukawa unification, in which the gluino is the next to lightest supersymmetric particle (NLSP). The NLSP gluino is slightly (∼10–30%) heavier than the LSP dark matter neutralino, and it primarily decays into the latter and a quark–antiquark pair or gluon. We find that NLSP gluino masses below ∼300 GeV are excluded by the ATLAS data. For LSP neutralino mass ∼200–300 GeV and $\mu > 0$, where μ is the coefficient of the MSSM Higgs bilinear term, the LHC constraints in some cases on the spin-dependent (spin-independent) neutralino–nucleon cross section are significantly more stringent than the expected bounds from IceCube DeepCore (Xenon 1T/SuperCDMS). For $\mu < 0$, this also holds for the spin-dependent cross sections.

1. Introduction

Low scale supersymmetry, augmented by an unbroken Z_2 matter (R-) parity, largely overcomes the gauge hierarchy problem encountered in the Standard Model (SM) and also provides a compelling cold dark matter candidate. In the mSUGRA/constrained minimal supersymmetric model (CMSSM) [1], as well as in many other realistic models, the lightest neutralino (LSP) is stable [2] with a relic density that is compatible with the WMAP dark matter measurements [3]. However, the small annihilation cross section of a pure bino LSP with mass of around 100 GeV does not permit one to easily reproduce the required relic dark matter abundance [4].

An interesting scenario which enhances the bino annihilation cross section is bino–gluino co-annihilation. In this case the bino and the relevant NLSP gluino (where NLSP stands for the next to lightest supersymmetric particle) are sufficiently close together in mass, such that the ensuing co-annihilation processes in the early universe allow one to reproduce the desired bino relic density. This scenario is not possible in the CMSSM, but it has been implemented in models with non-universal gaugino masses [5], and in a class of (third family) Yukawa unified models [6–8]. The collider signatures of the gluino co-annihilation scenario have recently been discussed in Refs. [9,10].

The ATLAS and CMS experiments at $\sqrt{s} = 7$ TeV LHC have previously presented their search results for low-energy supersymmetry corresponding to an integrated luminosity of 35 pb^{-1} [11,12], which was recently updated by ATLAS to 165 pb^{-1} [13]. The successful launch of the LHC and a flurry of supersymmetry related papers from the ATLAS and CMS Collaborations provides a strong impetus to explore regions of the MSSM parameter space not covered by the minimal version (CMSSM/mSUGRA). In this Letter we study the constraints and implications of recent LHC data on some well-motivated NLSP gluino models induced by gaugino mass non-universality and $t-b-\tau$ Yukawa coupling unification imposed at $M_{\rm GUT}$. The underlying symmetry group we consider is $SU(4)_c \times SU(2)_L \times SU(2)_R$ [14]. With the NLSP gluino and LSP neutralino having nearly degenerate masses, the chargino as well as leptons are absent in the gluino cascade decay. Also, the jets and missing energy from NLSP gluino decay are much softer due to the small mass difference between the NLSP and LSP. Thus, the conventional search strategy with same-sign chargino signature does not work here, and the usual requirement of large p_T jet and missing transverse momentum makes the event selection harder to implement. The LHC constraints on the NLSP gluino mass turn out to be significantly less restrictive than the recent 1 TeV or so mass bound on the gluino mass which, among other things, assume an essentially "massless" neutralino [13].

The Letter is organized as follows. In Section 2 we briefly summarize the NLSP gluino scenario with $t-b-\tau$ Yukawa unification and neutralino (essentially bino) dark matter. We also discuss the

* Corresponding author.
E-mail addresses: adeel@udel.edu (M.A. Ajaib), tli@udel.edu (T. Li), shafi@bartol.udel.edu (Q. Shafi).

0370-2693 © 2011 Elsevier B.V. Open access under CC BY license.
doi:10.1016/j.physletb.2011.09.083

NLSP gluino decay modes and outline the selection cuts employed by the ATLAS Collaboration. The results of two classes of NLSP gluino models constrained by the LHC data are presented together with a few benchmark points in Section 3. Our conclusions are summarized in Section 4.

2. NLSP gluino and ATLAS selection cuts

As mentioned earlier, the gluino–bino co-annihilation scenario requires the gluino to be NLSP in the sparticle spectrum, and to be nearly degenerate in mass with the bino LSP. The mass difference between the two should be [5]

$$\frac{M_{\tilde{g}} - M_{\tilde{\chi}_1^0}}{M_{\tilde{\chi}_1^0}} \lesssim 20\%. \tag{1}$$

In the framework of minimal supergravity, this feature clearly requires non-universal gaugino masses at $M_{\rm GUT}$. In particular, a partial unified model given by $SU(4)_c \times SU(2)_L \times SU(2)_R$ (4–2–2) group structure provides solutions to this scenario. Non-universal asymptotic gaugino masses are naturally accommodated in the supersymmetric 4–2–2 model and have recently been investigated in Refs. [6–8]. With the SM hypercharge in 4–2–2 given by $Y = \sqrt{2/5}(B-L) + \sqrt{3/5}I_{3R}$, one has the asymptotic relation between the three gaugino masses

$$M_1 = \frac{3}{5}M_2 + \frac{2}{5}M_3, \tag{2}$$

where M_1, M_2 and M_3 denote the asymptotic gaugino masses of $U(1)_Y$, $SU(2)_L \times SU(2)_R$ and $SU(3)_c$ respectively. Assuming that charged fermions of the third family acquires mass solely from a single $(1,2,2)$ representation in 4–2–2 leads to the Yukawa unification condition at $M_{\rm GUT}$ [15]

$$y_t = y_b = y_\tau \equiv y_{\rm Dirac}. \tag{3}$$

It has been shown that $t-b-\tau$ Yukawa unification can yield relatively light gluinos ($\leqslant 1$ TeV) [6,16].

In order to implement radiative electroweak breaking consistent with Yukawa unification, the soft mass terms of the two Higgs doublets must be non-universal at $M_{\rm GUT}$, such that the fundamental parameters in this class of models are

$$m_0, m_{H_u}, m_{H_d}, M_2, M_3, A_0, \tan\beta, \text{sign}(\mu). \tag{4}$$

Here m_0 is the universal soft mass of sfermions, A_0 is the universal trilinear scalar coupling, $\tan\beta$ is the ratio of the vacuum expectation values (VEVs) of the two MSSM Higgs doublets, and μ is the MSSM bilinear Higgs mass parameter. The software package ISAJET 7.80 [17] was employed in Refs. [6–8] to scan over the relevant parameter space, including renormalization group evolution of gauge and Yukawa couplings and all soft parameters, as well as the computation of the physical masses of all particles. A large number of relevant phenomenological constraints such as $BR(B_s \to \mu^+\mu^-)$ [18], $BR(b \to s\gamma)$ [19], $BR(B_u \to \tau\nu)$ [19], $\Delta(g-2)_\mu$ [20], WMAP relic density [3], LEP II bound on the lightest Higgs and all the sparticle mass bounds [21] are also implemented. The degree Yukawa of unification is quantified by the parameter R [22,6,7]

$$R \equiv \frac{\max(y_t, y_b, y_\tau)}{\min(y_t, y_b, y_\tau)}. \tag{5}$$

We shall require that $R \leqslant 1$, so that $t-b-\tau$ Yukawa unification holds at 10% level or better. Note that the NLSP gluino scenario with nearly-degenerate gluino and bino masses can be realized in 4–2–2 models for both $\mu > 0$ and $\mu < 0$ [6–8].

Because of the mass degenerate feature in Eq. (1), the NLSP gluino essentially decays into colored SM particles such as the gluon octet or a quark–antiquark pair, and the color singlet LSP $\tilde{\chi}_1^0$:

$$\tilde{g} \to q\bar{q}\tilde{\chi}_1^0, b\bar{b}\tilde{\chi}_1^0, g\tilde{\chi}_1^0, \tag{6}$$

where q ($\bar{q}$) denotes the first two generation quark (antiquark). The three-body decay $\tilde{g} \to q\bar{q}\tilde{\chi}_1^0, b\bar{b}\tilde{\chi}_1^0$ proceeds through an off-shell squark exchange, while the two-body decay $\tilde{g} \to g\tilde{\chi}_1^0$ involves a loop diagram containing squarks and quarks. The partial widths of these two decay channels are given by [23,24]

$$\begin{aligned}\Gamma\big(\tilde{g} \to g\tilde{\chi}_1^0\big) = {} & \frac{(M_{\tilde{g}}^2 - M_{\tilde{\chi}_1^0}^2)^3}{2\pi M_{\tilde{g}}^3}\Bigg[\frac{g_3^2 g_1}{128\pi^2}(M_{\tilde{g}} - M_{\tilde{B}}) \\ & \times \sum_q Q_q\left(\frac{1}{M_{\tilde{q}_L}^2} - \frac{1}{M_{\tilde{q}_R}^2}\right)N_{1B} \\ & + \frac{g_3^2 y_t^2}{32\sqrt{2}\pi^2 \sin\beta}\left(\frac{1}{M_{\tilde{q}_L}^2} + \frac{1}{M_{\tilde{u}_R}^2}\right) \\ & \times N_{1H_u} v\left(1 + \ln\frac{m_t^2}{M_{\tilde{g}}^2}\right)\Bigg]^2,\end{aligned} \tag{7}$$

$$\begin{aligned}\Gamma\big(\tilde{g} \to q\bar{q}\tilde{\chi}_1^0\big) = {} & \frac{M_{\tilde{g}}^5}{768\pi^3}\Bigg[\left(\frac{g_3 g_1}{6M_{\tilde{q}_L}^2}N_{1B} + \frac{g_3 g_2}{2M_{\tilde{q}_L}^2}N_{1W}\right)^2 \\ & + \left(\frac{2g_3 g_1}{3M_{\tilde{u}_R}^2}N_{1B}\right)^2 \\ & + \left(\frac{g_3 g_1}{6M_{\tilde{q}_L}^2}N_{1B} - \frac{g_3 g_1}{2M_{\tilde{q}_L}^2}N_{1W}\right)^2 \\ & + \left(\frac{g_3 g_1}{3M_{\tilde{d}_R}^2}N_{1B}\right)^2\Bigg] f\left(\frac{M_{\tilde{\chi}_1^0}}{M_{\tilde{g}}}\right) \quad (q = u, d),\end{aligned} \tag{8}$$

$$\begin{aligned}f(x) = {} & 1 + 2x - 8x^2 + 18x^3 - 18x^5 + 8x^6 - 2x^7 - x^8 \\ & - 12x^4 \ln x^2 + 12x^3(1 + x^2)\ln x^2.\end{aligned} \tag{9}$$

Here N_{1B}, N_{1W} and N_{1H_u} respectively denote the bino, wino and Higgsino components of the LSP neutralino $\tilde{\chi}_1^0$. Generally, the three-body decays will be suppressed if the scalar masses are too large, or by phase space if the mass difference between $\tilde{g}$ and $\tilde{\chi}_1^0$ ($\Delta M \equiv M_{\tilde{g}} - M_{\tilde{\chi}_1^0}$) is too small. Assuming $M_{\tilde{\chi}_1^0} \sim \mathcal{O}(250)$, together with the co-annihilation requirement in Eq. (1), one has the mass difference $\Delta M \simeq 50$ GeV. Also, for large $\tan\beta$, a large bottom Yukawa y_b naturally leaves the bottom squark (sbottom) to be the lightest squark, of $\mathcal{O}$ (TeV). With $\Delta M \simeq 50$ GeV and $\mathcal{O}$ (TeV) sbottom, $\tilde{g} \to b\bar{b}\tilde{\chi}_1^0$ decay often dominates. One can see this feature from Fig. 1 in Ref. [10], which shows the dependence of the gluino decay branching fraction in the $M_{\tilde{g}} - M_{\tilde{b}_1}$ plane for the 4–2–2 model with $\mu < 0$. The NLSP gluino decay is therefore sensitive to signals with multi-jets plus missing energy, and relatively more to final states with b-jets.

The ATLAS and CMS Collaborations have previously reported data in terms of events containing large missing transverse momentum and jets (with or without b-jets) in $\sqrt{s} = 7$ TeV proton–proton collisions, corresponding to an integrated luminosity of 35 pb^{-1}. No excess above the Standard Model (SM) background expectation was observed [11,12]. More recently, the ATLAS experiment has considered multi-jets plus missing energy events, with an integrated luminosity of 165 pb^{-1} [13]. With more strict selection cuts, new lower bounds on non-SM cross sections that are 30

Table 1
Summary of selection cuts and 95% C.L. upper limits on effective cross section for non-SM processes for signal regions S1, S2, S3 with 165 pb^{-1} luminosity, and region b with 35 pb^{-1} luminosity, following ATLAS data analyses [12,13].

	S1	S2	S3	b
Number of jets	$\geqslant 2$	$\geqslant 3$	$\geqslant 4$	$\geqslant 3$
Number of b-jets	0	0	0	$\geqslant 1$
Leading jet p_T (GeV)	> 130	> 130	> 130	> 120
Other jets p_T (GeV)	> 40	> 40	> 40	> 30
$\Delta\phi(\vec{p}_T^{\,\rm miss}, j_{1,2,3})$	> 0.4	> 0.4	> 0.4	> 0.4
$m_{\rm eff}$ (GeV)	> 1000	> 1000	> 1000	> 600
$\not{E}_T$ (GeV)	> 130	> 130	> 130	> 100
$\not{E}_T/m_{\rm eff}$	> 0.3	> 0.25	> 0.25	> 0.2
ATLAS $\sigma_{\rm exp}$ (pb)	0.035	0.03	0.035	0.32

times more stringent than from the 2010 data have been obtained. This analyse can also be employed, as we show here, to find useful constraints on NLSP gluino models with nearly degenerate gluino and LSP neutralino masses.

Note that gluino masses below 725 GeV are excluded at the 95% confidence level in simplified models containing only squarks of the first two generations, gluino and "massless" LSP neutralino [13]. In this case, with the gluino and squarks much heavier than LSP neutralino, the large mass difference results in highly energetic jets and large missing energy. With nearly-degenerate NLSP gluino and LSP neutralino, however, the jets from gluino decay and missing energy are softer, and fewer events with the same gluino mass would pass the same selection cuts. We therefore expect that the upper limit on the excluded gluino mass for degenerate NLSP gluino and LSP neutralino scenarios would be correspondingly lower.

The CMS analysis has stated less stringent constraints than ATLAS for low-energy supersymmetry search [25,26], and so we utilize the requirements used by ATLAS in our studies below. In the updated analysis for multi-jets and missing energy, the events are classified into 3 regions "S1", "S2" and "S3", where S1, S2, S3 require at least 2, 3, 4 jets respectively [13]. The second class of analysis requires at least one heavy flavor b-jet candidate in final states [12], denoted by "b" in the following. To simulate similar data, we generate all supersymmetric $2 \to 2$ events and include parton showering and hadronization using Pythia [27], and then forward them to fast detector simulation PGS-4 [28] to simulate the important detector effects. The b-tagging efficiency and mistagging rate in PGS-4 are based on the Technical Design Reports of ATLAS, and we use the default values in our analysis. We further follow the same ATLAS selection cuts for S1, S2, S3 and b. The cut requirements are summarized in Table 1, where $\Delta\phi(\vec{p}_T^{\,\rm miss}, j_{1,2,3})$ is the smallest azimuthal separation between the $\not{E}_T$ direction and the three leading jets, and $m_{\rm eff}$ is the scalar sum of $\not{E}_T$ and the transverse momenta of the highest p_T jets (up to two for region S1, three for region S2 and four for regions S3 and b respectively). The 95% C.L. upper limits on effective cross section (cross section times acceptance) for non-Standard Model (SM) processes for signal regions S1, S2, S3, b are also shown in Table 1. Following Ref. [26] we apply $\sigma \times$ acceptance $> \sigma_{\rm exp}$ as exclusion requirement for each model, where σ is the relevant total cross section and the acceptance is the ratio of signal events after and before selection cuts which reflects the effects of experimental efficiency.

3. LHC constraints on NLSP gluino and neutralino dark matter

3.1. $t - b - \tau$ Yukawa unification with $\mu < 0$

In Refs. [6,7], the supersymmetric 4–2–2 models with $t - b - \tau$ Yukawa unification are studied for positive [6] and negative [7] signs of the MSSM parameter μ. The $SU(2)_L$ gaugino mass M_2 was chosen to have the same sign as μ in order to remain consistent with the $(g-2)_\mu$ measurement. This is because the supersymmetric contribution to $(g-2)_\mu$ is proportional to μM_2. In this section we first consider the ATLAS constraints on 4–2–2 models with $\mu < 0$. In this case, the finite threshold correction to the Yukawa coupling y_b involving the gluino has the desired negative sign. Namely [29],

$$\delta y_b^{\text{SUSY-}finite} \approx \frac{g_3^2}{12\pi^2}\frac{\mu M_{\tilde g}\tan\beta}{M_b^2} + \frac{y_t^2}{32\pi^2}\frac{\mu A_t \tan\beta}{M_t^2}, \tag{10}$$

where g_3 is the strong gauge coupling, A_t is the stop trilinear coupling, and $M_b \approx (M_{\tilde b_1} + M_{\tilde b_2})/2$, $M_t \approx (M_{\tilde t_2} + \mu)/2$. For the desired Yukawa unification ($\approx 10\%$ or better), one obtains a wide range of acceptable gluino masses, namely $M_{\tilde g} \sim 250$ GeV and squark masses around 1 TeV, and heavier gluinos with $M_{\tilde g} \sim 1$ TeV as shown in Fig. 5 of Ref. [7]. In particular, for relatively light gluinos, Yukawa unification is compatible with the gluino–bino coannihilation mechanism and requires near-degenerate NLSP gluino and LSP neutralino masses.

To study the LHC constraints on this class of models, we generate about half a million models by scanning the parameter space [7] and finally obtain 5420 models after applying the various experimental constraints listed in Section 2. Out of these, 3945 models have acceptable Yukawa unification ($R \leqslant 1.1$), and in 3807 of these models gluino is the NLSP. The region in which the NLSP gluino and LSP neutralino are nearly mass degenerate corresponds to 250 GeV $\lesssim M_{\tilde g} \lesssim$ 300 GeV.

In Fig. 1 we show $\sigma \times$ acceptance vs. $M_{\tilde g}$ for 4–2–2 models with Yukawa unification and NLSP gluino, using the ATLAS regions S1, S2, S3 and b. The current experimental selections do not impose any constraints on heavier gluino solutions in this case. The near-degenerate NLSP–LSP points are also specified and actually overlap with the Yukawa unified points in the low gluino mass region. One can see that near-degenerate NLSP–LSP models with $M_{\tilde g} \lesssim 300$ GeV are essentially excluded. To display this perhaps more clearly, in Table 2 we outline the same number of excluded NLSP models with Yukawa unification as Fig. 1, and the excluded fraction for these models by the individual signal regions S1, S2, S3, b and combined S1, S2, S3, b. Among the three regions S1, S2, S3 of multi-jets plus missing energy final states, region S3 is the weakest for constraining NLSP gluino because it requires four jets with $p_T > 40$ GeV. However, the softest jet from a pair of NLSP gluinos more likely cannot have p_T more than about 20 GeV. Therefore, a greater number of events do not pass the selection cuts of region S3 compared with regions S1 and S2. Furthermore, as we expect, region b with b-jets in the final states excludes a significant fraction of NLSP gluino models, although we employ the early LHC data with 35 pb^{-1} integrated luminosity. This is because the decay $\tilde g \to b\bar b\tilde\chi_1^0$ is dominant in most of the NLSP gluino region, which makes the NLSP gluino models more sensitive to multi-b jets signature.

In Fig. 2 ($M_{\tilde g} - M_{\tilde\chi_1^0}$ plane), we display (in red color in the web version) the excluded models which have Yukawa unification and NLSP gluino. One can see that heavier gluinos (in blue color in the web version) with $M_{\tilde g} \gtrsim 500$ GeV are consistent with Yukawa unification, and being fairly massive, they survive the current LHC constraint.

It is important to see the implications of LHC data on direct and indirect dark matter detection in this class of Yukawa unified models with NLSP gluino. In Fig. 3 we display this by plotting the spin-independent and spin-dependent WIMP–nucleon scattering cross section $\sigma_{\rm SI}$ (left panel) and $\sigma_{\rm SD}$ (right panel) vs. $M_{\tilde\chi_1^0}$. A significant region around $M_{\tilde\chi_1^0} \simeq 200$ GeV is excluded by LHC

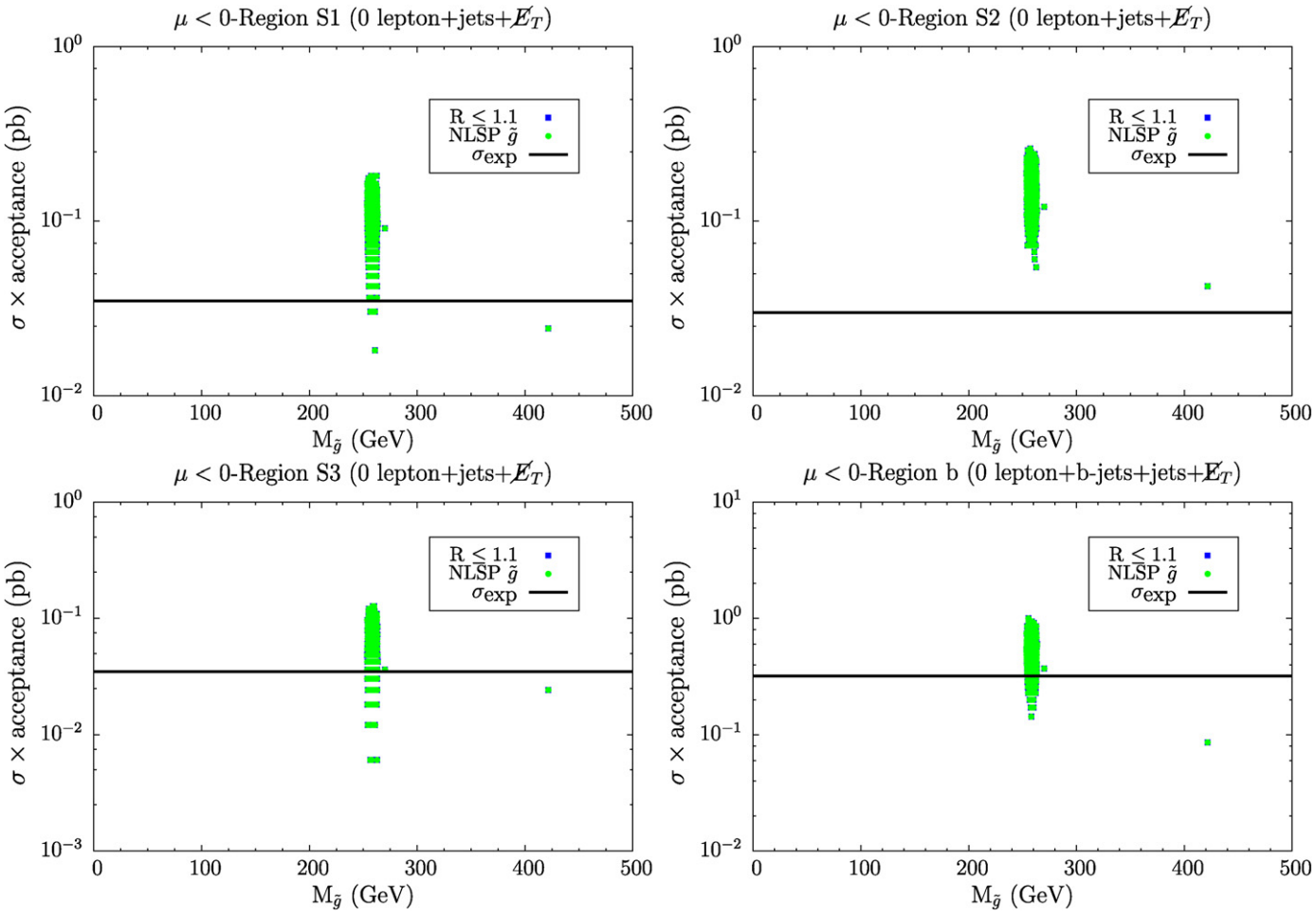

Fig. 1. $\sigma \times$ acceptance vs. $M_{\tilde{g}}$ with horizontal line as the 95% C.L. upper limits on effective cross section for non-SM processes for signal regions S1 (top left), S2 (top right), S3 (bottom left), b (bottom right) in the 4–2–2 framework with $\mu < 0$. Blue regions correspond to models with Yukawa unification ($R \leqslant 1.1$). NLSP gluino models form a subset of these and are represented by green points. (For interpretation of the references to color in this figure legend, the reader is referred to the web version of this Letter.)

Table 2
Number of excluded 4–2–2 models with Yukawa unification ($R \leqslant 1.1$) and NLSP gluino for $\mu < 0$. Also shown is the exclusion fraction by individual signal regions S1, S2, S3, b, and by combined S1, S2, S3, b.

$R \leqslant 1.1$ & NLSP $\tilde{g}$	S1	S2	S3	b	S1, S2, S3, b
Excluded	3800	3807	3385	3551	3807
Fraction	99.8%	100%	88.9%	93.3%	100%

data, although it is allowed by CDMS-II, XENON100, SuperK and IceCube experiments. This excluded region will be tested in the future by XENON 1T and SuperCDMS, but the region lies about three orders of magnitude below the expected IceCube DeepCore bound.

3.2. $t - b - \tau$ Yukawa unification with $\mu > 0$

With $\mu > 0$, the gluino contribution to $\delta y_b^{\text{finite}}$ is positive, so that the contribution from the chargino loop must be negative and sufficiently large in order to overcome this. In this scenario lower gluino masses and larger values of A_t and M_b in Eq. (10) are favored. All realistic NLSP gluino models compatible with the WMAP dark matter constraint give rise in this case to gluino masses in the range 220 GeV $\lesssim M_{\tilde{g}} \lesssim$ 400 GeV, with the LSP neutralino closely degenerate in mass. Also, because of the large A_t and M_b values, in this scenario one of the stops is usually the lightest squark, with the sbottom relatively heavier than in $\mu < 0$ case. Thus, the

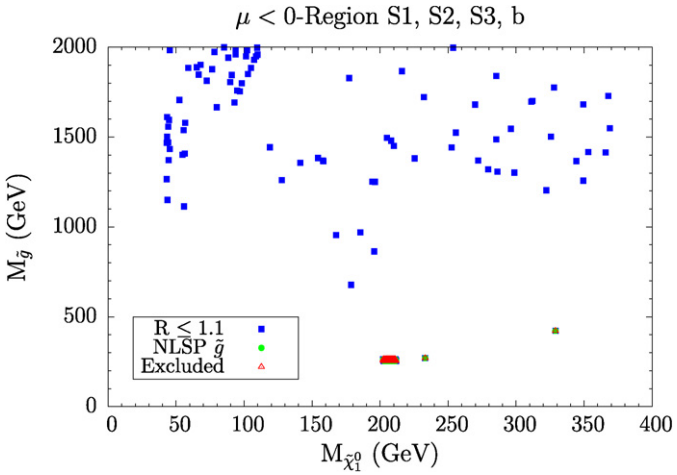

Fig. 2. $M_{\tilde{g}}$ vs. $M_{\tilde{\chi}_1^0}$ for models with Yukawa unification, NLSP gluino and those excluded models by ATLAS regions S1, S2, S3, b in the 4–2–2 framework with $\mu < 0$. Blue regions correspond to models with Yukawa unification ($R \leqslant 1.1$). Green regions are a subset with NLSP gluino, and models excluded by LHC data are in red color. (For interpretation of the references to color in this figure legend, the reader is referred to the web version of this Letter.)

three-body decay $\tilde{g} \to b\bar{b}\tilde{\chi}_1^0$ through an off-shell sbottom is suppressed, so that the constraint from b-jets in the final states is less

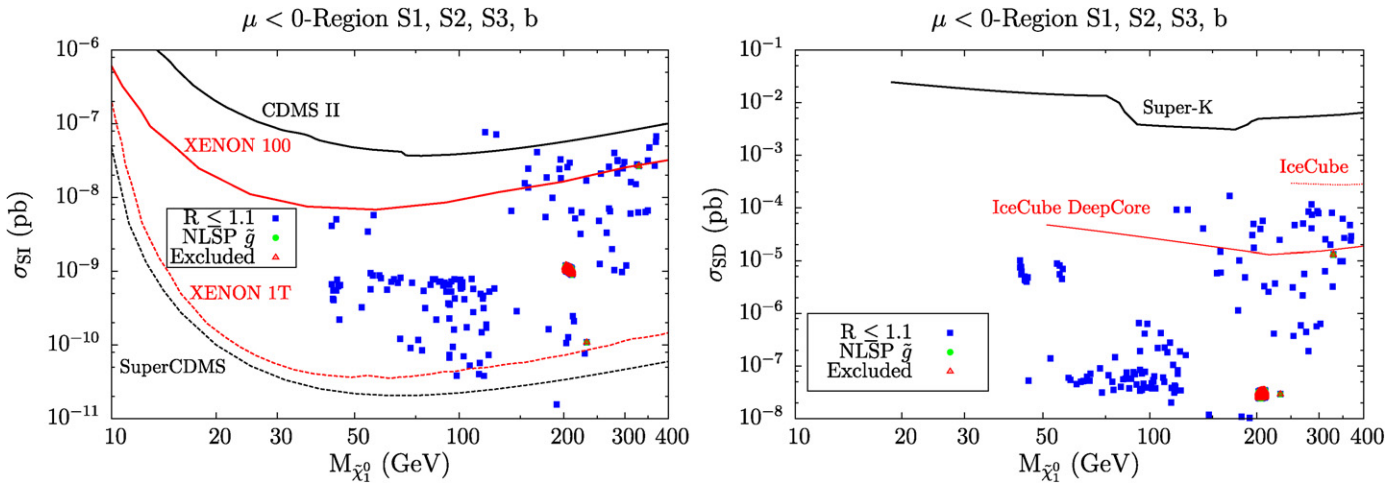

Fig. 3. $\sigma_{\rm SI}$ (left panel) and $\sigma_{\rm SD}$ (right panel) vs. $M_{\tilde{\chi}_1^0}$ in 4–2–2 models with Yukawa unification, NLSP gluino, and $\mu < 0$. The excluded region is denoted in red. The current limits from CDMS-II, XENON100, SuperK and IceCube and future projected sensitivities from XENON1T, SuperCDMS and IceCube DeepCore are also shown. (For interpretation of the references to color in this figure legend, the reader is referred to the web version of this Letter.)

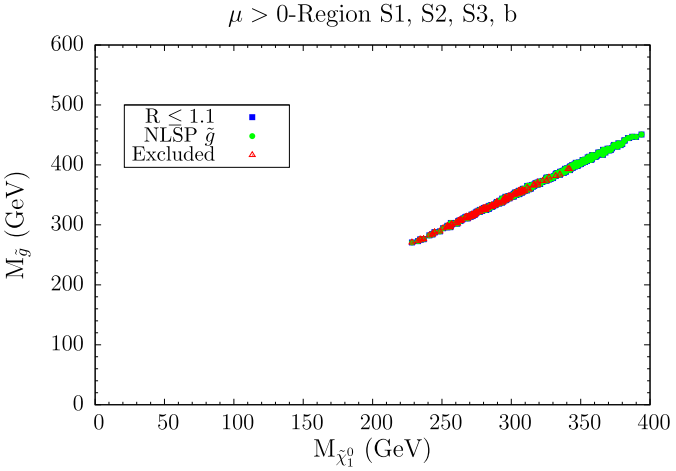

Fig. 4. $M_{\tilde{g}}$ vs. $M_{\tilde{\chi}_1^0}$ for models with Yukawa unification ($R \leqslant 1.1$, in blue), NLSP gluino (subset, in green) and those excluded by ATLAS regions S1, S2, S3, b (in red), for $\mu > 0$. (For interpretation of the references to color in this figure legend, the reader is referred to the web version of this Letter.)

stringent. We start with about 1 million models and obtain 17 942 models which survive the low-energy experiments. Out of these, about 400 models display acceptable Yukawa unification ($R \leqslant 1.1$) and contain NLSP gluino. Note that the constraint from $(g-2)_\mu$ is ignored in generating these models [7].

After applying the ATLAS selection cuts listed in Table 1 a significant number of models are excluded. We show this in Fig. 4 in the $M_{\tilde{g}} - M_{\tilde{\chi}_1^0}$ plane. The subset of models with NLSP gluino which overlaps with Yukawa unification is also specified. NLSP gluino masses below about 250–300 GeV are essentially excluded. In Fig. 5 we display the spin-independent and spin-dependent WIMP–nucleon scattering cross section $\sigma_{\rm SI}$ (left panel) and $\sigma_{\rm SD}$ (right panel) vs. $M_{\tilde{\chi}_1^0}$. One can see a significant region around $M_{\tilde{\chi}_1^0} \simeq 250$ GeV is excluded by the LHC data although it is allowed by CDMS-II, XENON100, SuperK and IceCube experiments. Indeed, some parts of the excluded parameter space lie beyond the reach of future experiments such as XENON 1T, SuperCDMS and IceCube DeepCore.

Finally, in Table 3 we present three characteristic benchmark points with NLSP gluino, dark matter neutralino and very acceptable $t-b-\tau$ Yukawa unification. Points 1 and 2, with gluino masses close to 300 GeV are excluded by the selection cuts listed in the table. However, point 3 with NLSP gluino mass close to 450 GeV and $M_{\tilde{g}} - M_{\tilde{\chi}_1^0} \sim 60$ GeV is compatible with the data. For $\mu > 0$ case, there are plenty of models with NLSP gluino mass above 400 GeV and nearly degenerate LSP neutralino, as shown in Fig. 4, thus evading the current ATLAS bounds based on the assumption of a "healthy" mass gap between the gluino and the LSP.

4. Summary

Inspired by the recent LHC search of final states containing jets and/or b-jet and missing transverse momentum, corresponding to an integrated luminosity of 165 pb^{-1}, we have explored its ramifications for supersymmetric $SU(4)_c \times SU(2)_L \times SU(2)_R$ models which display $t-b-\tau$ Yukawa unification at 10% level or better, contain NLSP gluino, and possess LSP neutralino dark matter. The experimental simulation typically assumes a healthy mass gap between the gluino and the rest of the SUSY spectrum, particularly the LSP, such that the excluded gluino mass limit is about 700 TeV. In the NLSP gluino scenario we expect the bounds to weaken because of the small mass difference between the NLSP gluino and LSP neutralino. The NLSP gluino primarily decays into the LSP neutralino and a gluon or quark–antiquark pair, thus allowing us to exploit this LHC data. For $\mu < 0$, the NLSP gluino mass spectra with good Yukawa unification has $M_{\tilde{g}} \sim 250$ GeV and squark masses around 1 TeV, as well as heavier gluino solutions with $M_{\tilde{g}} \sim 1$ TeV. We generate about 4000 models for this case, from an initial half a million models, which satisfy the above criteria of Yukawa unification, NLSP gluino, and neutralino dark matter, after imposing constraints from all previous experiments (except LHC). The $\mu > 0$ case has NLSP gluino with $220 \lesssim M_{\tilde{g}} \lesssim 400$ GeV, but it is not compatible with the $(g-2)_\mu$ constraint. The corresponding number of models for $\mu > 0$ is around 400. We next show that for closely mass degenerate NLSP gluino and LSP neutralino, models with NLSP gluino masses below 300 GeV or so are largely excluded by the LHC data. Because of the relatively small gluino pair production cross section, gluinos with $M_{\tilde{g}} \gtrsim 500$ GeV in $\mu < 0$ case ($M_{\tilde{g}} \gtrsim 400$ GeV in $\mu > 0$ case) survive the current LHC selection requirement as shown in blue in the web version in Fig. 2 (models in green in the web version in Fig. 4 and point 3 in Table 3). The LHC implications for spin-dependent and spin-independent LSP neutralino–nucleon cross sections are also explored. Regions

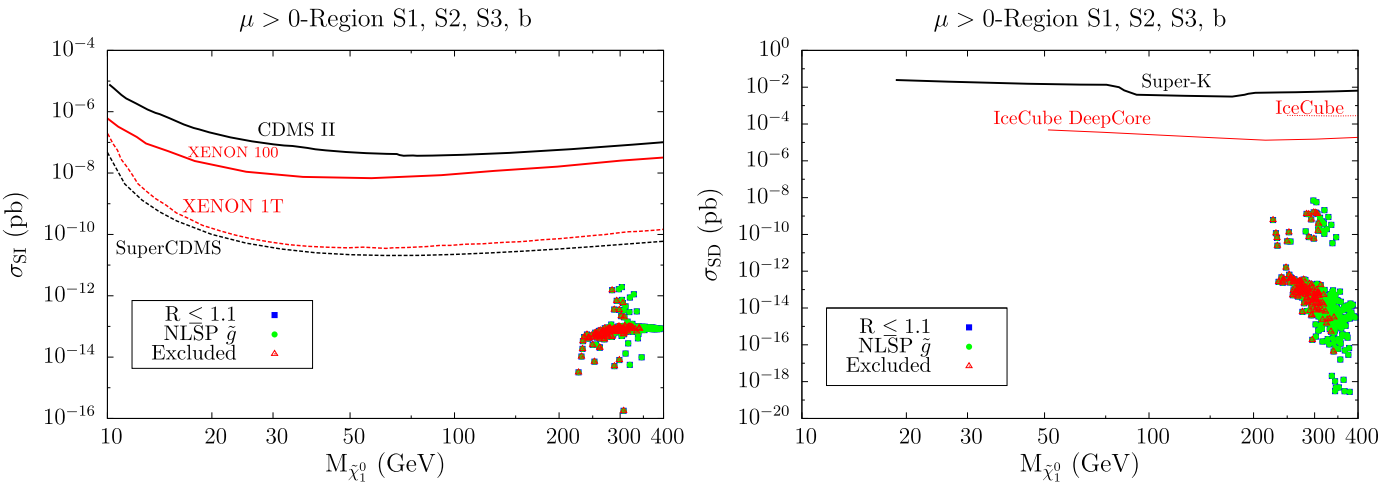

Fig. 5. σ_{SI} (left panel) and σ_{SD} (right panel) vs. $M_{\tilde{\chi}_1^0}$. Color scheme is the same as in Fig. 3. The current limits from CDMS-II, XENON100, SuperK and IceCube and future anticipated bounds from XENON1T, SuperCDMS and IceCube DeepCore are also shown. (For interpretation of the references to color in this figure legend, the reader is referred to the web version of this Letter.)

Table 3
LHC limits on three NLSP gluino benchmark points that satisfy all the experimental constraints described in Section 2. Various selection cuts from the four signal regions, namely, S1, S2, S3 and b exclude point 1, whereas point 2 is excluded by the first two regions. Point 3 is allowed by all four signal regions.

	Point 1	Point 2	Point 3
m_0	1511	10317	19639
M_1	−468.24	436.59	672.06
M_2	−826.2	719.35	1119.4
M_3	68.7	12.45	1.05
$\tan\beta$	47.5	49.66	50.93
A_0	−1680.23	−24285	−49722
sgn(μ)	−1	+1	+1
m_{Hu}	505.5	3550.53	7964.78
m_{Hd}	1029.83	10288.17	16115.48
m_h	114	125	126
m_H	445	6307	6631
m_A	442	6266	6588
$m_{H^\pm}$	454	6308	6632
$m_{\tilde{\chi}^0_{1,2}}$	202, 684	237, 737	390, 1204
$m_{\tilde{\chi}^0_{3,4}}$	1136, 1144	10231, 10231	20043, 20043
$m_{\tilde{\chi}^\pm_{1,2}}$	685, 1144	740, 10218	1208, 20037
$m_{\tilde{g}}$	258	276	447
$m_{\tilde{u}_{L,R}}$	1595, 1503	10323, 10155	19649, 19482
$m_{\tilde{t}_{1,2}}$	996, 1163	4291, 4712	6887, 7953
$m_{\tilde{d}_{L,R}}$	1597, 1515	10324, 10381	19649, 19728
$m_{\tilde{b}_{1,2}}$	971, 1172	4384, 4715	7717, 8379
$m_{\tilde{\nu}_1}$	1595	10222	19550
$m_{\tilde{\nu}_3}$	1416	7785	15082
$m_{\tilde{e}_{L,R}}$	1597, 1533	10221, 10526	19547, 19861
$m_{\tilde{\tau}_{1,2}}$	1119, 1421	4850, 7775	9338, 15025
σ_{SI} (pb)	1.14×10^{-9}	4.48×10^{-14}	8.17×10^{-14}
σ_{SD} (pb)	3.06×10^{-8}	2.60×10^{-13}	3.52×10^{-15}
$\Omega_{CDM}h^2$	0.11	0.10	0.09
R	1.04	1.08	1.04
$\sigma\times$ acc (S1) (pb)	0.133	0.073	0.012
$\sigma\times$ acc (S2) (pb)	0.158	0.048	0.018
$\sigma\times$ acc (S3) (pb)	0.091	0.03	0.006
$\sigma\times$ acc (b) (pb)	0.6	0.2	0

of the parameter space, some lying well below the much anticipated future bounds from IceCube DeepCore and Xenon 1T and SuperCDMS, are already excluded by utilizing the LHC data.

Acknowledgements

We would like to thank Gregg Peim, Bin He, Ilia Gogoladze, Rizwan Khalid and Shabbar Raza for useful discussions. This work is supported by the DOE under grant No. DE-FG02-91ER40626.

References

[1] A. Chamseddine, R. Arnowitt, P. Nath, Phys. Rev. Lett. 49 (1982) 970;
R. Barbieri, S. Ferrara, C. Savoy, Phys. Lett. B 119 (1982) 343;
N. Ohta, Prog. Theor. Phys. 70 (1983) 542;
L.J. Hall, J.D. Lykken, S. Weinberg, Phys. Rev. D 27 (1983) 2359;
For a review see: H.P. Nilles, Phys. Rep. 110 (1984) 1;
S. Weinberg, The Quantum Theory of Fields: Vol. 3, Supersymmetry, Cambridge University Press, 2000, 442 pp.
[2] For a review see: G. Jungman, M. Kamionkowski, K. Griest, Phys. Rep. 267 (1996) 195.
[3] E. Komatsu, et al., WMAP Collaboration, Astrophys. J. Suppl. 192 (2011) 18.
[4] S. Profumo, C.E. Yaguna, Phys. Rev. D 70 (2004) 095004.
[5] S. Profumo, C.E. Yaguna, Phys. Rev. D 69 (2004) 115009.
[6] I. Gogoladze, R. Khalid, Q. Shafi, Phys. Rev. D 79 (2009) 115004.
[7] I. Gogoladze, R. Khalid, S. Raza, Q. Shafi, arXiv:1008.2765 [hep-ph].
[8] I. Gogoladze, R. Khalid, S. Raza, Q. Shafi, arXiv:1102.0013 [hep-ph].
[9] D. Feldman, Z. Liu, P. Nath, Phys. Rev. D 80 (2009) 015007;
D.S.M. Alves, E. Izaguirre, J.G. Wacker, arXiv:1102.5338 [hep-ph].
[10] M.A. Ajaib, T. Li, Q. Shafi, K. Wang, JHEP 1101 (2011) 028.
[11] G. Aad, et al., ATLAS Collaboration, arXiv:1102.5290 [hep-ex].
[12] G. Aad, et al., ATLAS Collaboration, arXiv:1103.4344 [hep-ex].
[13] ATLAS Collaboration, ATLAS-CONF-2011-086.
[14] J.C. Pati, A. Salam, Phys. Rev. D 10 (1974) 275.
[15] B. Ananthanarayan, G. Lazarides, Q. Shafi, Phys. Rev. D 44 (1991) 1613;
B. Ananthanarayan, G. Lazarides, Q. Shafi, Phys. Lett. B 300 (1993) 245;
Q. Shafi, B. Ananthanarayan, Trieste HEP Cosmol. (1991) 233.
[16] H. Baer, S. Kraml, S. Sekmen, H. Summy, JHEP 0803 (2008) 056;
H. Baer, M. Haider, S. Kraml, S. Sekmen, H. Summy, JCAP 0902 (2009) 002.
[17] H. Baer, F.E. Paige, S.D. Protopopescu, X. Tata, arXiv:hep-ph/0001086.
[18] T. Aaltonen, et al., CDF Collaboration, Phys. Rev. Lett. 100 (2008) 101802.
[19] E. Barberio, et al., Heavy Flavor Averaging Group, arXiv:0808.1297 [hep-ex].
[20] G.W. Bennett, et al., Muon G-2 Collaboration, Phys. Rev. D 73 (2006) 072003.
[21] S. Schael, et al., Eur. Phys. J. C 47 (2006) 547.
[22] H. Baer, S. Kraml, S. Sekmen, H. Summy, JHEP 0803 (2008) 056;
H. Baer, M. Haider, S. Kraml, S. Sekmen, H. Summy, JCAP 0902 (2009) 002.
[23] P. Gambino, G.F. Giudice, P. Slavich, Nucl. Phys. B 726 (2005) 35, arXiv:hep-ph/0506214.
[24] M. Toharia, J.D. Wells, JHEP 0602 (2006) 015, arXiv:hep-ph/0503175.
[25] S. Akula, N. Chen, D. Feldman, M.X. Liu, Z.W. Liu, P. Nath, G. Peim, Phys. Lett. B 699 (2011) 377;
S. Akula, D. Feldman, Z.W. Liu, P. Nath, G. Peim, arXiv:1103.5061 [hep-ph].
[26] T.J. LeCompte, S.P. Martin, arXiv:1105.4304 [hep-ph].
[27] T. Sjostrand, S. Mrenna, P.Z. Skands, JHEP 0605 (2006) 026.
[28] John Conway, http://www.physics.ucdavis.edu/~conway/research/software/pgs/pgs4-general.htm.
[29] I. Gogoladze, S. Raza, Q. Shafi, arXiv:1104.3566 [hep-ph].